Journal of the European Ceramic Society xxx (xxxx) xxx–xxx

Contents lists available at ScienceDirect

Journal of the European Ceramic Society

journal homepage: www.elsevier.com/locate/jeurceramsoc

Original Article

Effect of temperature and stoichiometry on the long-range 1:2 cation order in $BaZn_{1/3}Ta_{2/3}O_3$

Taras Kolodiazhnyi[a,*], Jintara Padchasri[b], Rattikorn Yimnirum[b]

[a] National Institute for Materials Science, 1-1 Namiki, Tsukuba, Ibaraki 305-0044, Japan
[b] School of Physics, Institute of Science and NANOTEC-SUT COE on Advanced Functional Nanomaterials, Suranaree University of Technology, Nakhon Ratchasima 30000, Thailand

ARTICLE INFO

Keywords:
Complex perovskites
Non-stoichiometry
Phase transitions
Microwave dielectric resonators

ABSTRACT

We report on the compositional stability range, the degree of atomic order and Raman and optical spectra of the off-stoichiometric $BaZn_{1/3}Ta_{2/3}O_3$ (BZT) within the BaO–ZnO–Ta_2O_5 ternary diagram. Almost all off-stoichiometric BZT compositions equilibrated at 1200 °C show significant degree of the long-range 1:2 cation order ranging from 60% to 80%. Ceramics equilibrated at 1550 °C and annealed at 1450 °C show strong effect of composition on the 1:2 order. The regions where an 1:2 atomic order is robust to the deviation from stoichiometry include the off-stoichiometric compositions along the BZT–$Ba_4Ta_2O_9$, BZT–$Ba_3Ta_2O_8$, BZT–$BaTa_2O_6$, BZT–Ta_2O_5, BZT–$ZnTa_2O_6$ and BZT–$Zn_4Ta_2O_9$ (pseudo) tie lines. At the same time ceramics formulated along the BZT–BaO, BZT–ZnO, BZT–$BaZnO_2$, BZT–Ba_2ZnO_3 tie lines and BZT–'Ba_3ZnO_4' pseudo tie line show complete disorder. There is a very close correlation between the degree of the 1:2 order on one hand and the unit cell volume and lattice distortion on the other hand. The ordered BZT show contraction of the unit cell whereas disordered ceramics show expansion of the unit cell in the off-stoichiometric region. The pronounced signatures of the order-disorder phase transition in the Raman and optical spectra are discussed.

1. Introduction

The problem of 1:2 *B*-site cation order–disorder transition in perovskite $Ba(B'_{1/3}B''_{2/3})O_3$, where B′ and B″ are di- and penta-valent cations, respectively, has been studied by both theoretical [1–5] and experimental [6–14] methods. Electrostatic (Coulomb) force that drives the *B*-site cation ordering in $Ba(B'_{1/3}B''_{2/3})O_3$ is proportional to $1/\varepsilon$, where ε is the static dielectric constant [1]. As such, the $Ba(B'_{1/3}B''_{2/3})O_3$ niobates that have higher ε disorder more easily than tantalates, whereas the high-ε $Pb(B'_{1/3}B''_{2/3})O_3$ perovskites do not show 1:2 order at all.

Beside the exposure to high-temperature there are other ways to disorder the $Ba(B'_{1/3}B''_{2/3})O_3$ perovskites. The 1:2 *B*-site order in $Ba(B'_{1/3}B''_{2/3})O_3$ can be destroyed by partial substitution with alio-valent cations. For example, $(1-x)BaMg_{1/3}Ta_{2/3}O_3$-$xBaSnO_3$, $(1-x)BaMg_{1/3}Nb_{2/3}O_3$-$xBaSnO_3$ and $(1-y)BaMg_{1/3}Ta_{2/3}O_3$-$yBaTiO_3$ alloys disorder at $x \geq 0.1$ and $y \geq 0.15$, respectively [8,15,16]. Similarly, in the (1-*x*)$BaZn_{1/3}Ta_{2/3}O_3$-$xBaZrO_3$ the disorder sets on at $x \approx 0.04$ [17]. The 1:2 order in the (1-*x*)$BaZn_{1/3}Ta_{2/3}O_3$-$xSrGa_{1/2}Ta_{1/2}O_3$ solid solution disappears at $x \geq 0.1$ [18], whereas in the (1-*x*) $BaZn_{1/3}Ta_{2/3}O_3$-$xZrO_2$ ceramics the 1:2 cation order is destroyed at $x \geq 0.015$ [19]. The Raman spectra and powder X-ray diffraction of (1-*x*)$BaZn_{1/3}Ta_{2/3}O_3$-$xBaGa_{1/2}Ta_{1/2}O_3$ ceramics sintered between 1450–1600 °C show complete disorder for $x = 0.05$ [20].

Cation disorder in $Ba(B'_{1/3}B''_{2/3})O_3$ can also be induced by intrinsic point defects formed as a result of the deviation from ideal stoichiometry. According to Koga et al. [10,11], partial disorder has been found in $BaZn_{1/3}Ta_{2/3}O_3$ with a small deviation towards the Ba-rich composition. Similar trend was found by Surendran et al. [9] for Ba-rich $BaMg_{1/3}Ta_{2/3}O_3$ perovskite. Later on, Wu and Davies reported complete disorder in Ba-rich and Nb-deficient $BaZn_{1/3}Nb_{2/3}O_3$ ceramics [21], whereas Belous et al. [13], Ovchar et al. [12] and Sayyadi-Shahraki et al. [14] have found similar trends in $BaMg_{1/3}Nb_{2/3}O_3$ and $BaCo_{1/3}Nb_{2/3}O_3$ perovskites. Partial disorder in Ba-rich $BaMg_{1/3}Ta_{2/3}O_3$ has been reported in Ref. [22].

It is widely accepted that the 1:2 *B*-site order in $Ba(B'_{1/3}B''_{2/3})O_3$ ceramics critically affects the microwave dielectric loss [23–25]. Therefore, understanding the factors and mechanisms that drive the order-disorder phase transition is important from both the academic and industrial perspectives. There are very few studies of the off-stoichiometric $BaZn_{1/3}Ta_{2/3}O_3$, hereafter abbreviated as BZT. According to the subsolidus BaO–ZnO–Ta_2O_5 phase diagram reported by Vanderah

* Corresponding author.
E-mail address: kolodiazhnyi.taras@nims.go.jp (T. Kolodiazhnyi).

https://doi.org/10.1016/j.jeurceramsoc.2017.11.048
Received 1 October 2017; Received in revised form 15 November 2017; Accepted 22 November 2017
0955-2219/ © 2017 Elsevier Ltd. All rights reserved.

Please cite this article as: Kolodiazhnyi, T., Journal of the European Ceramic Society (2017), https://doi.org/10.1016/j.jeurceramsoc.2017.11.048

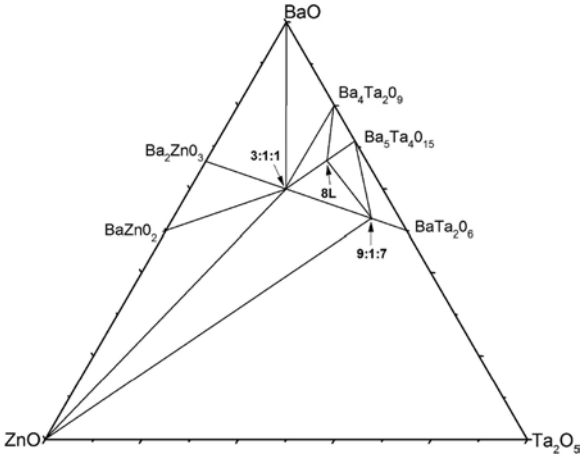

Fig. 1. Part of the BaO–ZnO–Ta_2O_5 subsolidus phase diagram. Pseudo-ternary phases: $Ba_3ZnTa_2O_9$, $Ba_8ZnTa_6O_{24}$ and $Ba_9ZnTa_{14}O_{45}$ are labeled as 3:1:1, 8 L and 9:1:7, respectively. The Ta_2O_5-rich part of the phase diagram is omitted for clarity.

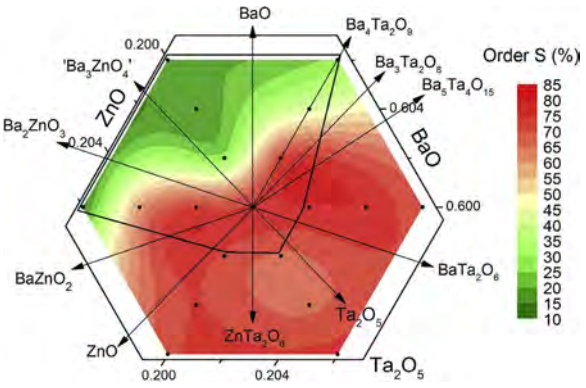

Fig. 2. Enlarged part of Fig. 1 in the vicinity of the BZT composition that shows the order parameter of the off-stoichiometric BZT equilibrated at 1400 °C for 100 h adapted from Koga et al. [10]. The black line polygon outlines the single-phase region. The axis numbers are the mole fractions of the corresponding oxides labeled in large font.

et al. [26], BZT forms seven tie lines with pseudo-binary and pseudo-ternary compounds (Fig. 1). These include: BZT – $Ba_9ZnTa_{14}O_{45}$, BZT – $Ba_8ZnTa_6O_{24}$, BZT – $Ba_4Ta_2O_9$, BZT – BaO, BZT – Ba_2ZnO_3, BZT – $BaZnO_2$ and BZT – ZnO. The pseudo-ternary phase with approximate composition of $Ba_9ZnTa_{14}O_{45}$ belongs to the tetragonal tungsten bronze (TTB) structure first reported by Kryshtop et al. [27], whereas the $Ba_8ZnTa_6O_{24}$ is a hexagonal 8-layer perovskite first reported by Tolmer and Desgardin [28] and solved by Moussa et al. [29]. Furthermore, we cannot rule out two more BZT tie lines with metastable $Ba_3Ta_2O_8$ and $Ba_6Ta_2O_{11}$ phases reported by Kovba et al. [30,31] although the existence of the latter phases has been questioned by Vanderah et al. [32]. The most detailed study of the BZT off-stoichiometry and the 1:2 order disorder was reported by Koga et al. [10] for ceramics sintered at 1400 °C. Their data adapted from Ref. [10] are shown in Fig. 2. While the high degree of the 1:2 order in the Ta-rich and Ba-deficient regions of the off-stoichiometric BZT can be understood in terms of the point defect model of Wu and Davies [21], the existence of the long range 1:2 cation order in the Ba-deficient and Zn-rich regions (Fig. 2) are at odds with the order–disorder interpretation proposed in Ref. [21]. Given the industrial importance of these ceramics [23], we felt it necessary to explore the order-disorder phase transition in the off-stoichiometric BZT in more detail.

2. Experimental

Around 95 chemical compositions with different xBaO–yZnO–$z$$Ta_2O_5$ ratios were prepared from well-dried $BaCO_3$ (99.9%, Wako Chemicals), ZnO (99.9%, Wako Chemicals) and Ta_2O_5 (99.9%, Kanto Kagaku Reagents). The powders were mixed in ethanol with zirconia balls on rollers at 80 rpm for 20 h. After drying at 60 °C the powders were screened through the 100-mesh nylon sieve and compressed into pucks of 25 mm diameter under 500 kg/cm^2 pressure in tungsten carbide (WC) pressing die. The pucks were calcined in air at 1200 °C for 5 h in 99.6% pure alumina crucibles covered with alumina lids. Care was taken to avoid cross-contamination of the pucks and to minimize the loss of ZnO during heat-treatment. After calcination, the powders were re-milled at the same conditions, mixed with polyvinyl alcohol binder, screened through the 100-mesh nylon sieve and compacted into pellets of 7 mm diameter and 3 mm thickness under uniaxial 1000 kg/cm^2 pressure in WC pressing die. The compacted pellets were heat treated under two different conditions: (i) 1200 °C for 5 h and (ii) 1550 °C for 10 h followed by anneal at 1450 °C for 20 h. Finally both sets of samples were cooled down to room temperature at 1000 °C/h.

Phase purity and lattice parameters of the ceramic specimens were analyzed by powder X-ray diffraction (PXRD) (Miniflex 600 diffractometer with Cu K_α X-ray source, Rigaku, Japan). To minimize the second phases that form on the surface of the ceramic pucks, prior to X-ray diffraction, the outer surface of the sintered ceramics was ground with abrasive paper. This usually helped to reduce the surface second phase contamination in the powder X-ray diffraction patterns. The structural parameters were obtained from Rietveld refinement of the X-ray data by using JANA2006 program [33]. Lattice parameters and Wyckoff site and atomic fractional coordinates were initiated by using the BZT structural data from Ref. [34] The diffraction profiles were refined in the range of $10^\circ < 2\theta < 140^\circ$. During refinement, atomic thermal factors, B, for weak X-ray scattering elements such as, O1(3e), O2(6i) and Zn(1b) were fixed, while the B factors for Ba1(1a), Ba2(2d) and Ta(2d) were relaxed and successfully refined to positive values. To estimate the degree of B-site cation disorder, the occupancies of the B-site cations were relaxed under constraint g[Zn(1b)] × 1 + g[Zn (2d)] × 2 = 1 and g[Ta(1b)] × 1 + g[Ta(2d)] × 2 = 2, where g is the fractional occupancy of the ion whose Wyckoff site is shown in brackets.

Although the above approach worked well for highly ordered BZT compositions, it was found that the majority of the non-stoichiometric BZT samples had significant degree of disorder with rather broad ± 1/3{hkl} supercell reflections due to the small size of the 1:2 ordered domains. These latter cases were rather difficult to refine using a single histogram approach because of the very different peak profiles for sub- and super-cell reflections. Similar problem has been also reported by Reaney et al. [34]. Therefore, in this study a 'brute force' method was used to achieve a more systematic estimate of the order parameter. The order parameter, S, was deduced from the ratio of the X-ray integrated intensity of the strongest supercell peak, (100), to the integrated intensity of the main peak of the BZT structure. The 1:2 order parameter is given by

$$S = \sqrt{\frac{(I_{100}/I_{110,012,102})_{obs}}{(I_{100}/I_{110,012,102})_{calc}}}, \quad (1)$$

where $(I_{100}/I_{110,012,102})_{obs}$ is the ratio of the observed integrated intensity of the (100) supercell reflection to that of (110,012,102) main reflection, and $(I_{100}/I_{110,012,102})_{calc} \approx 0.037$ is the calculated value for a completely ordered BZT structure.

Microstructure and phase assemblage of the polished ceramics were examined with Hitachi S-4800 scanning electron microscope equipped with energy dispersive X-ray spectrometer (HORIBA Emax) and YAG backscattered electron detector. Room temperature Raman spectra (Jobin Yvon/Horiba) of the fine-polished sample surface were measured in the backscattered geometry in the 30–1200 cm^{-1} frequency range with Ar–Kr 514.5 nm laser. Room temperature optical absorption

in the visible and UV spectral range (250–850 nm) was measured with JASCO V-7200 spectrometer. The dense ceramic samples were thinned down to the thickness of 30–50 μm using an automatic polishing/grinding machine. At the final step, the thinned discs of 6 mm diameter were polished with 1 μm diamond slurry to achieve a mirror quality surface. The absorption coefficient was calculated from the measured optical absorbance and the thickness of the sample.

3. Results and discussion

3.1. Phase equilibria and defect solubility

In preparation of the off-stoichiometric BZT we have used the pseudo-ternary BaO–ZnO–Ta_2O_5 phase diagram shown in Fig. 1 as a guide. However, the existence of one more pseudo-ternary phase, i.e., $Ba_2ZnTaO_{5.5}$, with partially 1:1 ordered perovskite structure (F m$\bar{3}$m space group) is controversial [21]. While Jacobson et al. [35] have reported the latter phase, Vanderah et al. [32] have not included $Ba_2ZnTaO_{5.5}$ in the BaO–ZnO–Ta_2O_5 subsolidus (Fig. 1). To clarify this controversy we have attempted to prepare $Ba_2ZnTaO_{5.5}$ in this study. The target composition of $Ba_2ZnTaO_{5.5}$ was equilibrated at 1200 °C for 10 h with one intermediate re-grinding. The resulting product was a mixture of two phases: disordered BZT and $BaZnO_2$ crystallized in the $P3_121$ space group with $a = b = 5.8496(2)$ Å and $c = 6.7544(3)$ U +00C5. The cell parameters of the $BaZnO_2$ determined here were close to that of the $a = 5.886$ U+00C5 and $c = 6.734$ U+00C5 reported by von Schnering et al. [36]. Therefore, in agreement with the results of Vanderah et al. [26], we could not confirm the existence of the 1:1 ordered $Ba_2ZnTaO_{5.5}$ phase.

To obtain a more detailed map of the off-stoichiometric BZT we have included in our study four hypothetical tie-lines: BZT–Ta_2O_5, BZT–$ZnTa_2O_6$, BZT–'$Zn_4Ta_2O_9$' and BZT–'Ba_3ZnO_4'. Furthermore, to clarify some important trends in the off-stoichiometric regions we have also studied several BZT compositions away from the tie lines.

The approximate boundary region of the single phase off-stoichiometric BZT equilibrated at 1200 °C determined by the PXRD is outlined by the solid line in Fig. 3a. It is in qualitative agreement with the data reported in Ref. [10]. The prominent exception is the BaO-rich compositions along the BZT – BaO tie line. In contrast to Koga et al. [10], our study indicates extremely small defect solubility along the BZT – BaO tie line (Fig. 4) with the secondary phases composed primarily of the $Ba_4Ta_2O_9$ polymorphs. For BZT equilibrated at 1200 and 1550 °C the secondary phases along the BZT – xBaO tie line are detected for $x \geq 0.005$ and 0.01, respectively as shown in Fig. 4. The differences between our results and the data reported by Koga et al. [11] may be explained by the sublimation of BaO at high temperatures. Indeed during the thermal equilibration of Ba-rich BZT at 1400 °C for 100 h reported in Ref. [11] most of the excess BaO may have been lost due to the sublimation. This may give a misleading impression of the extended single phase region along the BZT – BaO tie line.

As for the rest of the off-stoichiometric compositions, in good agreement with Refs. [10,11] the single phase regions along the BZT–$x Ba_4Ta_2O_9$ tie line (Fig. 5), BZT – $x Ba_3Ta_2O_8$ pseudo tie line (Fig. 1 in Ref. [37]) and BZT – $x BaTa_{4/5}O_3$ tie line (Fig. 2 in Ref. [37]) extend to $x \approx 0.01$, 0.016 and 0.07, respectively [37]. The solubility of point defects along the BZT – $x BaTa_2O_6$ tie line (Fig. 3 in Ref. [37]) and BZT – $x Ta_2O_5$ pseudo tie line (Fig. 4 in Ref. [37]) does not exceed $x \approx 0.01$ and 0.007, respectively. The single phase regions along the BZT – $x ZnTa_2O_6$ (Fig. 4), BZT – xZnO (Fig. 1 in Ref. [37]), BZT – $x Ba_2ZnO_3$ (Fig. 3 in Ref. [37]) and BZT – $x BaZnO_2$ (Fig. 5 in Ref. [37]) tie lines extend to $x \approx 0.0035$, 0.01, 0.02 and 0.03, respectively.

As evidenced by the PXRD profiles, most of the off-stoichiometric BZT ceramics sintered at 1550 °C and annealed at 1450 °C show some traces of the $Ba_8ZnTa_6O_{24}$ 8-layer hexagonal perovskite phase. The SEM examination of the polished BZT samples with small deviation from the stoichiometric composition did not show this second phase, however. We conclude, therefore, that this phase forms on the surface of the sintered ceramics due to Zn evaporation and could not be avoided in the PXRD patterns.

The deviation from stoichiometry impacts the microstructure of the sintered ceramics. The BZT ceramics formulated close to the stoichiometric composition showed rather regular grain distribution with an average grain size of 8–10 μm (Fig. 6a). BZT ceramics in the Zn-deficient and Ba-deficient regions of the phase diagram showed some needle-like and plate-like second phases formed on the surface of the thermally etched samples (Fig. 6b). These second phases are identified as $Ba_8ZnTa_6O_{24}$ 8-layer hexagonal perovskite and $Ba_9ZnTa_{14}O_{45}$ tetragonal tungsten bronzes. In contrast, ceramics in the Zn-rich and Ta-deficient parts of the phase diagram showed an evidence of the large irregular-shaped grains formed during the liquid-phase assisted grain growth (Fig. 6c and d).

3.2. Effect of composition and temperature on the 1:2 cation order

Both temperature and off-stoichiometry have profound effect on the 1:2 cation order in BZT. The B-site 1:2 order parameter for BZT equilibrated at 1200 °C is mapped in Fig. 3. An important result is that all of the BZT non-stoichiometric compositions equilibrated at 1200 °C show partial order of ≈60–80%. The highest degree of 1:2 order was detected for Zn-deficient and Ta-rich compositions along the BZT–$Ba_3Ta_2O_8$, BZT–$Ba_5Ta_4O_{15}$, BZT–$BaTa_2O_6$ tie lines as well as along the BZT–Ta_2O_5 pseudo tie line. Remarkably, partial 1:2 order of ≈60–70% was also detected in the BZT–Ba_2ZnO_3 and BZT–$BaZnO_2$ joints (Fig. 3a).

For ceramics equilibrated at 1550 °C and annealed at 1450 °C for 20 h, an increase in the 1:2 cation order of up to $S \approx 95$–100% was detected in the off-stoichiometric BZT formulated along the BZT–$Ba_4Ta_2O_9$ (Fig. 5b), BZT–$Ba_3Ta_2O_8$ (Fig. 1 Ref. [37]), BZT–$Ba_5Ta_4O_{15}$ (Fig. 2 Ref. [37]), BZT–$BaTa_2O_6$ (Fig. 3 Ref. [37]) and BZT–Ta_2O_5 (Fig. 4 Ref. [37]) tie lines (also see Fig. 3b). These results

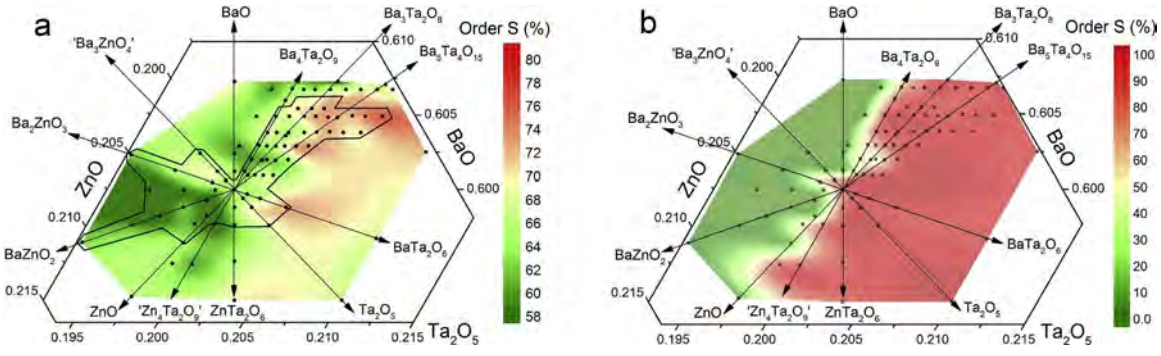

Fig. 3. B-site 1:2 cation order parameter in the vicinity of the BZT equilibrated at 1200 °C for 5 h (a) and BZT sintered at 1550 °C for 10 h and annealed at 1450 °C for 20 h (b). The single phase region, as determined by powder XRD is outlined by a solid line. Please note a different scale of the S parameter in panels (a) and (b).

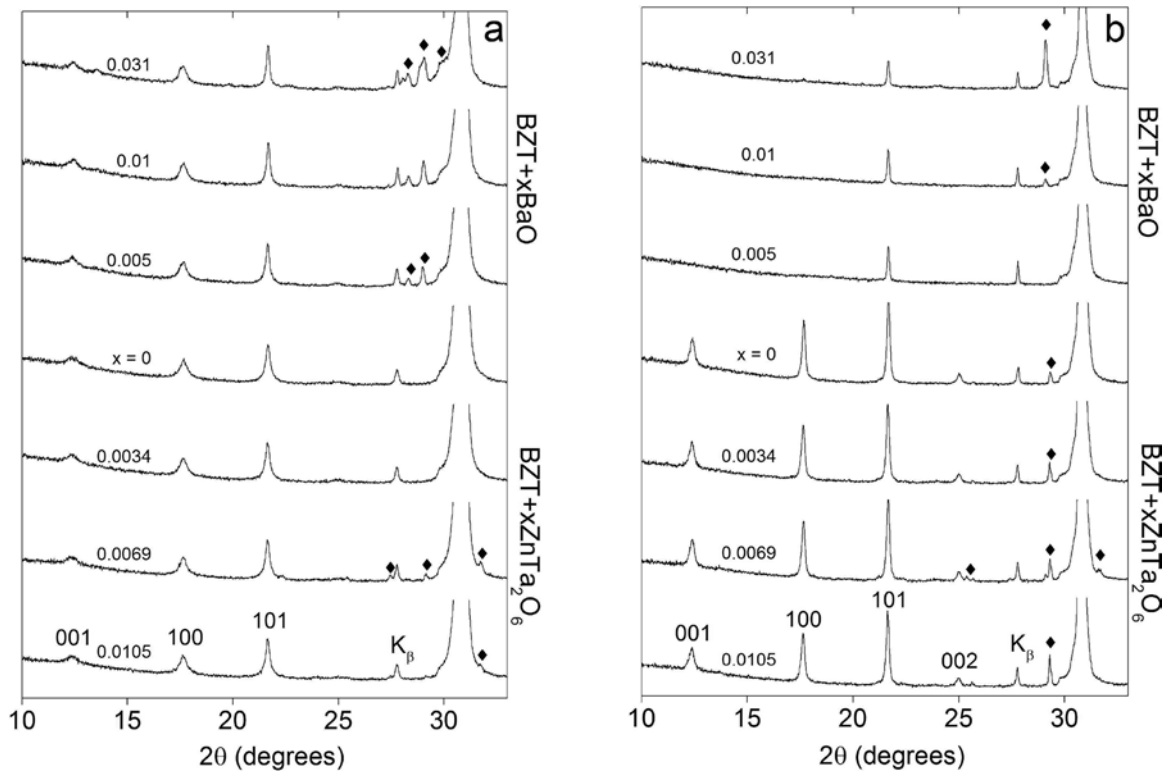

Fig. 4. Powder XRD profiles for ceramics formulated along the BZT-*x*BaO (BaO-rich) and BZT-*x*$ZnTa_2O_6$ (BaO-deficient) tie lines and equilibrated at (a) 1200 °C for 5 h and (b) 1550 °C for 10 h followed by anneal at 1450 °C for 20 h. The diamonds indicate the $BaCO_3$ and $Ba_4Ta_2O_9$ second phase polymorphs for BZT-*x*BaO joint and $Ba_9ZnTa_{14}O_{45}$ TTB second phase for the BZT-*x*$ZnTa_2O_6$ joint. Traces of the $Ba_8ZnTa_6O_{24}$ second phase were detected in stoichiometric BZT and in BaO-deficient ceramics sintered at 1550 °C as discussed in the text.

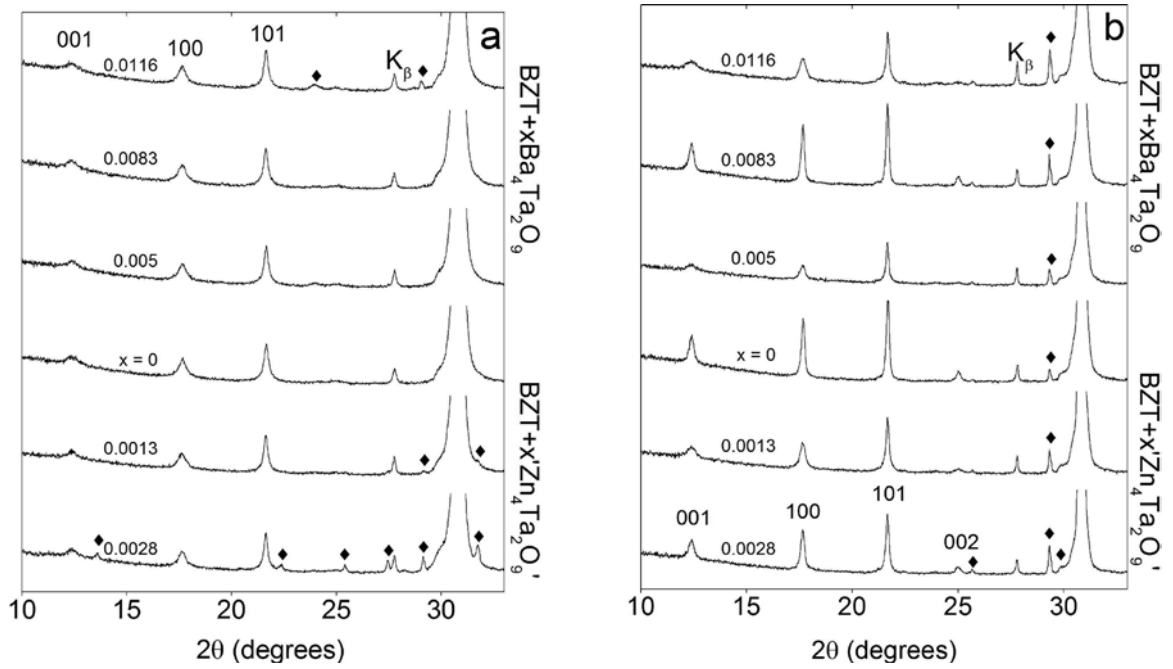

Fig. 5. Powder XRD profiles for $Ba_4Ta_2O_9$-rich and '$Zn_4Ta_2O_9$'-rich BZT equilibrated at (a) 1200 °C for 5 h and (b) 1550 °C for 10 h followed by anneal at 1450 °C for 20 h. The diamonds indicate the $Ba_4Ta_2O_9$ second phase polymorphs along the $Ba_4Ta_2O_9$-rich compositions and $Ba_9ZnTa_{14}O_{45}$ TTB second phase for '$Zn_4Ta_2O_9$'-rich compositions, respectively.

are in good agreement with the BZT data reported in Ref. [10] as well as with the $BaMg_{1/3}Ta_{2/3}O_3$ data [22]. For Nb-based analogues, i.e., $BaZn_{1/3}Nb_{2/3}O_3$ and $BaCo_{1/3}Nb_{2/3}O_3$ an increase in the 1:2 order parameter was reported upon deviation from the ideal stoichiometry towards the $Ba_5Nb_4O_{15}$ phase [13,14,21].

While the high-temperature anneal at 1450 °C has brought an increase in the 1:2 order in some Zn-deficient and Ta-rich parts of the BaO–ZnO–Ta_2O_5 subsolidus, the opposite trend has been detected in the other parts of the phase diagram (Fig. 3b). In particular, the long-range 1:2 order is destroyed along the BZT–BaO tie line (Fig. 4b). After the high-temperature anneal, the long-range 1:2 order disappears in the Ta-deficient BZT along the BZT–'Ba_3ZnO_4' pseudo tie line(Fig. 4 in Ref.

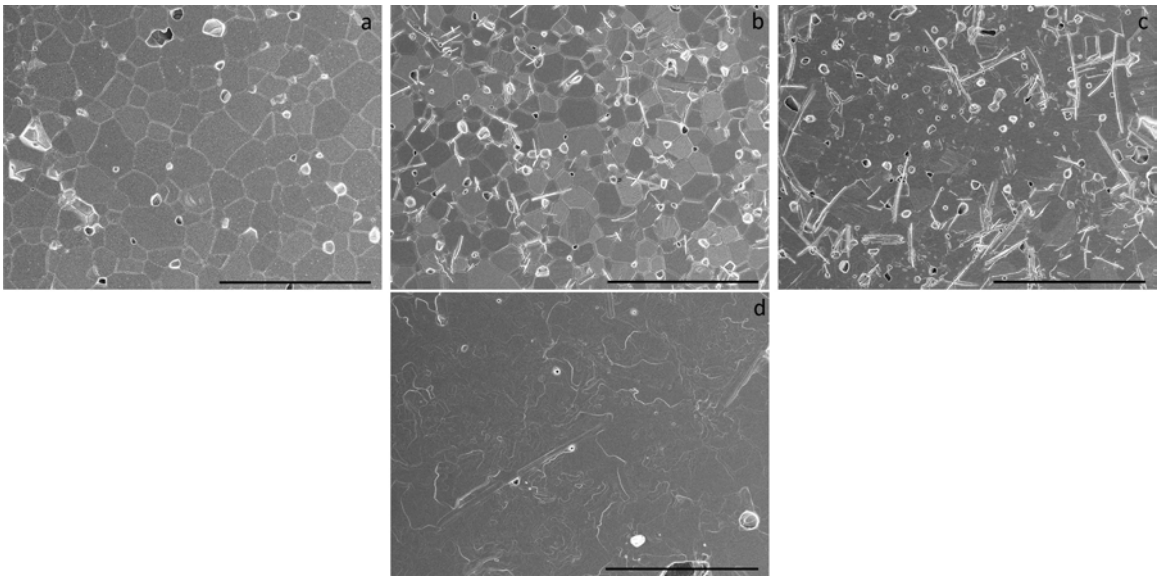

Fig. 6. SEM micrographs of polished and thermally etched surfaces of BZT sintered at 1550 °C for 10 h followed by anneal at 1450 °C for 20 h: Stoichiometric BZT (a), BZT – 0.002 $ZnTa_2O_6$ (b), BZT – 0.012 Ba_2ZnO_3 (c), BZT – 0.02 ZnO (d). The horizontal black line indicates a 50 μm scale.

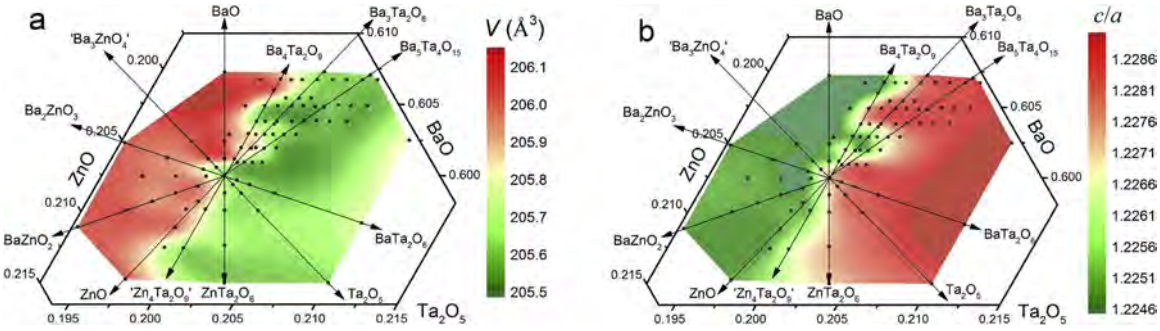

Fig. 7. Unit cell volume (a) and *c/a* ratio (b) of BZT sintered at 1550 °C and annealed at 1450 °C for 20 h. The axis numbers are the mole fractions of the corresponding oxides labeled in large font.

[37]). Significant suppression of the 1:2 order has been also detected in the Zn-rich region along the BZT–ZnO and BZT–$BaZnO_2$ tie lines (Figs. 3b and Figs. 1 and 5 in Ref. [37]). Similar drop in the 1:2 order parameter in this composition region has been reported for BZT [11], $BaCo_{1/3}Nb_{2/3}O_3$ [14] and $BaZn_{1/3}Nb_{2/3}O_3$ [21].

It is important to note that the BZT–$Ba_4Ta_2O_9$ tie line represents rather sharp boundary between the ordered and disordered BZT (Fig. 3b). In fact, few compositions along this line accidentally show disorder: For example, ceramics with the BZT – 0.002 $Ba_4Ta_2O_9$ composition in Fig. 5b shows disordered PXRD pattern. We explain this by experimental error during the preparation of the target composition located on the tie line. Similar compositional sensitivity to the long-range 1:2 order along the $BaMg_{1/3}Ta_{2/3}O_3$–$Ba_4Ta_2O_9$ tie line has been encountered by one of the authors during the study of the off-stoichiometric $BaMg_{1/3}Ta_{2/3}O_3$ [22]. We conclude that the small deviation from the BZT–$Ba_4Ta_2O_9$ tie line towards the BaO-BZT-$Ba_4Ta_2O_9$ compositional triangle (see Fig. 1) results in the drastic loss of the 1:2 cation order.

Several attempts have been made in the past to find a link between the point defect chemistry and the order-disorder transition in the non-stoichiometric $Ba(B'_{1/3}B''_{2/3})O_3$ [21,25]. First, Desu and O'Bryan [25] have assumed that during the prolonged thermal anneal of the BZT ceramics at 1300 °C, the loss of Zn results in the formation of the antisite Ba_{Zn} defects. The authors of Ref. [25] have found that this process is accompanied by an increase in the *c/a* lattice distortion which promotes the 1:2 ordering and enhances the microwave quality factor. This hypothesis was later dismissed by Wu and Davies during the studies of the non-stoichiometric $BaZn_{1/3}Nb_{2/3}O_3$: They demonstrated that the ceramics formulated along the $BaZn_{1/3}Nb_{2/3}O_3$–$Ba(Ba_{1/3}Nb_{2/3})O_3$ tie line are disordered [21]. Similar to $BaZn_{1/3}Nb_{2/3}O_3$, the non-stoichiometric $BaCo_{1/3}Nb_{2/3}O_3$ compositions formulated along the $BaCo_{1/3}Nb_{2/3}O_3$–$xBa(Ba_{1/3}Nb_{2/3})O_3$ tie line show complete disorder [14]. It seems, however, that these results cannot be extrapolated to the Ta-based systems: The non-stoichiometric $BaMg_{1/3}Ta_{2/3}O_3$ ceramics show an enhanced degree of the 1:2 order along the $BaMg_{1/3}Ta_{2/3}O_3$–$Ba(Ba_{1/3}Ta_{2/3})O_3$ tie line [22]. In the present study, ceramics formulated along the BZT–$Ba(Ba_{1/3}Ta_{2/3})O_3$ tie line also show a very high degree of the 1:2 order (Figs. 3 and 5). Obviously, the Nb- and Ta-based $Ba(B'_{1/3}B''_{2/3})O_3$ perovskites show very different cation ordering behavior in this off-stoichiometric region. The reasons for such a difference are not clear yet and require further studies.

3.3. Unit cell volume and lattice distortion of non-stoichiometric BZT

As revealed in Fig. 7, the unit cell volume and *c/a* lattice distortion are very closely related to the degree of the long range 1:2 cation order in BZT (Fig. 3). As the 1:2 order increases, the unit cell contracts (Fig. 7a) and the *c/a* lattice parameter ratio becomes larger than $\sqrt{3/2} \approx 1.2247$ (Fig. 7b).

Burton and Cockayne [4] have identified two driving forces that govern the order/disorder process in the $A(B'_{1/3}B''_{2/3})O_3$ perovskites with heterovalent B-site cations. These are (i) long-range Coulomb

interactions that 'maximize the unlike charges on the nearest-neighbour *B*-sites' and (ii) short-range interactions associated with the optimization of the *A*–O bonds. The long-range Coulomb interactions are working to eliminate the strongly underbonded oxygens in the Zn^{2+}–O–Zn^{2+} linear triplets in BZT that may only form in the (partially) disordered structure [4]. In contrast, in Pb-based $A(B'_{1/3}B''_{2/3})O_3$ perovskites, the occurrence of the Zn^{2+}–O–Zn^{2+} triplets is compensated by the enhanced Pb–O bonding to the underbonded oxygens which destabilizes the 1:2 ordered ground state [4].

Manifestation of the short-range interactions in $Ba(B'_{1/3}B''_{2/3})O_3$ that operate to optimize the bond valence sums has been discussed in detail by Lufaso [38]. In the 1:2 ordered BZT, the underbonded Ta^{5+} ions undergo an off-center shift toward the face of the TaO_6 octahedra closer to the neighboring layers of ZnO_6 octahedra [38] in such a way that Ta^{5+} forms three short and three long bonds with the oxygen ligands [39]. The overall result of this bond strain is a decrease in the unit cell volume in the 1:2 ordered BZT. Disorder lifts the crystal symmetry, destroys the correlated off-center displacement of the Ta^{5+} ions and brings the formation of the Zn^{2+}–O–Zn^{2+} triplets which ultimately leads to an increase in the unit cell volume. The strongest lattice contraction and the highest *c/a* ratio were found along the BZT–$Ba_5Ta_4O_{15}$ and the BZT–$Ba_3Ta_2O_8$ (pseudo) tie lines as well as in the BZT–$Ba_5Ta_4O_{15}$–$BaTa_2O_6$ and BZT–$Ba_5Ta_4O_{15}$–$Ba_3Ta_2O_8$ compositional triangles (Fig. 7).

3.4. Raman and optical signatures of the 1:2 cation order in BZT

The Raman spectra for the two BZT ceramics sintered at 1550 °C and annealed at 1450 °C are shown in Fig. 8. The ordered BZT was formulated along the BZT–$Ba_5Ta_4O_{15}$ tie line whereas the disordered BZT was formulated along the BZT–Ba_2ZnO_3 tie line. The Raman spectrum of the 1:2 ordered BZT closely resembles the one reported in Ref. [40]. According to the $BaZn_{1/3}Ta_{2/3}O_3$ space group symmetry, there are 9 Raman active vibrational modes. Their accurate assignment to the normal vibrations of the specific Ba, Ta and O atoms has been reported by Chia et al. [41]. The lowest energy $A_{1g} + E_g$ split mode ($104 + 107\ cm^{-1}$) is attributed to the normal vibrations of the Ba atoms with 2*d* site symmetry against the oxygen octahedra. The three weak phonons at 157, 212 and 260 cm^{-1} are associated with the E_g(O), E_g(Ta) and A_{1g}(Ta) modes, respectively, and are closely related to the 1:2 order [42]. The phonons at 377 and 425 cm^{-1} are due to the A_{1g}(O) + E_g(O) and E_g(O) modes of vibrations, respectively. The strong phonon at 808 cm^{-1} is due to the A_{1g}(O) stretch mode of the oxygen octahedra originating from the oxygen atoms with the 6*i* site symmetry [41].

The loss of the long range 1:2 order has profound effect on the BZT Raman spectrum (Fig. 8). The A_{1g}(Ba) + E_g(Ba) mode at 105 cm^{-1} shows large broadening accompanied by the formation of the low- and high-energy shoulders at 85 and 119 cm^{-1}, respectively. The three 1:2 order-related modes at 157–260 cm^{-1} range are absent in the disordered BZT. The O-related F_{2g}(O) and E_g(O) modes found in the 1:2 ordered BZT at 377 and 425 cm^{-1}, respectively, spread in energy from 362 to 440 cm^{-1} and become suppressed (Fig. 8). Finally, the most intense A_{1g}(O) mode shifts to lower energy (792 cm^{-1}) and develops a low-energy shoulder at ≈739 cm^{-1}. Its full width at half maximum (FWHM) increases from 27 cm^{-1} for ordered BZT to 35 cm^{-1} for disordered one. It is interesting to note that the very similar Raman spectrum has been reported for disordered $La_xBa_{1-x}Zn_{(1+x)/3}Ta_{(2-x)/3}O_3$ with $x = 0.02$ [43]. Both the peak broadening and the slight decrease in the energy of the phonons can be intuitively understood in terms of an increase in the anharmonic contribution to the lattice potential as the BZT undergoes transition from the ordered to the disordered phase accompanied by a slight expansion of the unit cell.

Very little is known about the optical band gap of the BZT. Kim has reported the optical band gap of the 1:2 ordered BZT at $E_g \approx 4.32$ eV determined by the diffuse reflectance spectroscopy [44]. To the best of our knowledge, no optical band gap data were reported for disordered BZT. In this study we used the direct optical absorption method that allows quantitative analysis of the optical data. The optical absorption coefficients of the ordered stoichiometric BZT and the disordered BZT ceramics are shown in Fig. 9. According to the data, the optical band gaps of the 1:2 ordered and disordered BZT are estimated at $E_g \approx 4.60$ and 4.16 eV, respectively. The E_g of the ordered BZT is 0.44 eV larger than that of the disordered one. It is also worth noting that the absorption coefficient away from the band gap is almost identical for both ceramics and is not far from the value of $180 \pm 50\ cm^{-1}$ reported for Ni-doped BZT [45].

4. Concluding remarks

The long-rage 1:2 order in BZT shows very strong compositional and temperature dependence. For ceramics sintered at 1550 °C and annealed at 1450 °C, a rather sharp boundary along the '$Zn_4Ta_2O_9$'–BZT–$Ba_4Ta_2O_9$ (pseudo) tie line separates the 1:2 ordered and disordered BZT compositions. The remarkable feature of this tie

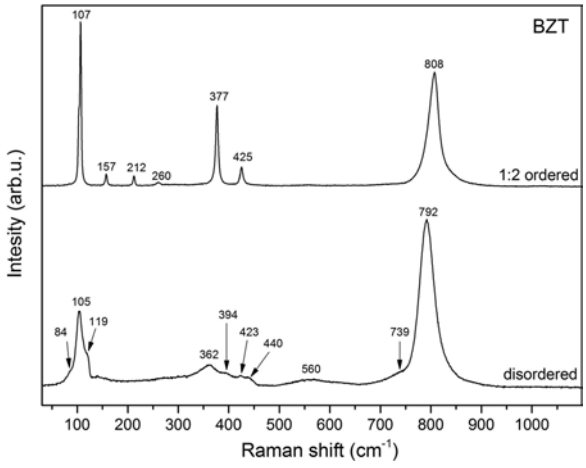

Fig. 8. Raman spectra of the 1:2 ordered and disordered BZT ceramics sintered at 1550 °C and annealed at 1450 °C for 20 h.

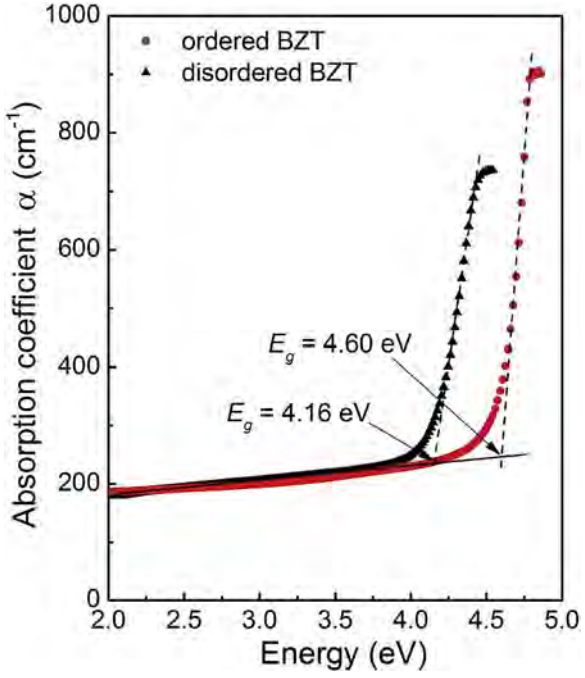

Fig. 9. Optical absorption coefficient of the 1:2 ordered and disordered BZT ceramics sintered at 1550 °C and annealed at 1450 °C for 20 h.

line is that it separates the Ta-rich compounds from the Ta-deficient ones. Similar to the non-stoichiometric $BaMg_{1/3}Ta_{2/3}O_3$ compounds [22], the BZT compounds formulated along this tie line show the 1:2 ordered ground state. Slight deviation from this boundary towards the Ta-deficient compositions results in the loss of the 1:2 order in BZT. It is tempting to assign the Ta-related point defect, such as $[V_{Ta}–V_O]$ complex, to be responsible for the order-disorder transition in $Ba(B'_{1/3}B''_{2/3})O_3$. However, it is important to note that the Nb-based analogue of the BZT is disordered along the $BaZn_{1/3}Nb_{2/3}O_3–Ba_4Nb_2O_9$ tie line [21] which requires further studies and precludes us from making a far-reaching conclusions about the exact nature of the point defects responsible for the 1:2 order-disorder in the $Ba(B'_{1/3}B''_{2/3})O_3$ compounds.

Acknowledgements

This work was supported by JSPS Grant-in-Aid for Scientific Research26400323. J.P. work at NIMS was supported by the Science Achievement Scholarship of Thailand (SAST). Motivating discussions with Hitoshi Ohsato, Takeshi Shimada and Robert Freer are gratefully acknowledged. T.K. also thanks R&D staff of Com Dev Int. including Ming Yu, William Fitzpatrick and Antonio Panariello for their active interest in this work.

Appendix A. Supplementary data

Supplementary data associated with this article can be found, in the online version, at http://dx.doi.org/10.1016/j.jeurceramsoc.2017.11.048.

References

[1] L. Bellaiche, D. Vanderbilt, Electrostatic model of atomic ordering in complex perovskite alloys, Phys. Rev. Lett. 81 (1998) 1318–1321.
[2] L. Bellaiche, J. Padilla, D. Vanderbilt, Heterovalent and A-atom effects in $A(B'B'')O_3$ perovskite alloys, Phys. Rev. B 59 (1999) 1834–1839.
[3] B.P. Burton, Empirical cluster expansion models of cation order-disorder in $A(B'_{1/3}B''_{2/3})O_3$ perovskites, Phys. Rev. B 59 (1999) 6087–6091.
[4] B.P. Burton, E. Cockayne, Why $Pb(BB')O_3$ perovskites disorder at lower temperatures than $Ba(BB')O_3$ perovskites? Phys. Rev. B 60 (1999) R12542–R12545.
[5] T. Takahashi, First-principles investigation of the phase stability for $Ba(B'^{2+}_{1/3}B''^{5+}_{2/3})O_3$ microwave dielectrics with the complex perovskite structure, Jpn. J. Appl. Phys. 39 (2000) 5637–5641.
[6] R. Guo, A.S. Bhalla, L.E. Cross, $BaMg_{1/3}Ta_{2/3}O_3$ single crystal fiber grown by the laser heated pedestal growth technique, J. Appl. Phys. 75 (1994) 4704–4708.
[7] L. Chai, M.A. Akbas, P.K. Davies, J.B. Parise, Cation ordering transformations in $BaMg_{1/3}Ta_{2/3}O_3$-$BaZrO_3$ perovskite solid solutions, Mater. Res. Bull. 32 (1997) 1261–1269.
[8] L. Chai, P.K. Davies, Effect of M^{4+} (Ce, Sn, Ti) B-site substitutions on the cation ordering in $BaMg_{1/3}Ta_{2/3}O_3$, Mater. Res. Bull. 33 (1998) 1283–1292.
[9] K.P. Surendran, M.T. Sebastian, P. Mohanan, R.L. Moreira, A. Dias, Effect of non-stoichiometry on the structure and microwave dielectric properties of Ba$(Mg_{0.33}Ta_{0.67})O_3$, Chem. Mater. 17 (2005) 142–151 and references therein.
[10] E. Koga, H. Moriwake, K. Kakimoto, H. Ohsato, Influences of composition deviation from stoichiometric $BaZn_{1/3}Ta_{2/3}O_3$ on superlattice ordering and microwave quality factor Q, J. Ceram. Soc. Jpn. 113 (2005) 172–178.
[11] E. Koga, Y. Yamagishi, H. Moriwake, K. Kakimoto, H. Ohsato, Large *Q* factor variation within dense, highly ordered $Ba(Zn_{1/3}Ta_{2/3})O_3$ system, J. Eur. Ceram. Soc. 26 (2006) 1961–1964.
[12] O. Ovchar, D. Durylin, A. Belous, B. Jancar, T. Kolodiazhnyi, A-site deficient perovskites $Ba(M^{2+}_{1/3}Nb_{2/3})O_3$: microstructural attributes for a high quality factor, Mater. Sci. Pol. 29 (2011) 56–62.
[13] A.G. Belous, O.V. Ovchar, A.V. Kramarenko, B. Jancar, J. Bezjak, D. Suvorov, Effect of nonstoichiometry on the structure and microwave dielectric properties of $BaCo_{1/3}Nb_{2/3}O_3$, Inorg. Mater. 46 (2010) 529–533.
[14] A. Sayyadi-Shahraki, E. Taheri-Nassaj, J. Gonzales, N. Newman, T. Kolodiazhnyi, Effect of non-stoichiometry on the densification, phase purity, microstructure, crystal structure, and dielectric loss of $BaCo_{1/3}Nb_{2/3}O_3$ ceramics, J. Eur. Ceram. Soc. 37 (2017) 3335–3346.
[15] J. Zhang, Y. Zhou, Z. Yue, X. Zhang, L. Li, Microwave dielectric properties and thermally stimulated depolarization currents of $(1-x)Ba(Mg_{1/3}Nb_{2/3})O_3$-$xBaSnO_3$ solid solutions, J. Am. Ceram. Soc. 98 (2015) 3942–3947.
[16] L.-C. Tien, C.-C. Chou, D.-S. Tsai, Microstructure of $BaMg_{1/3}Ta_{2/3}O_3$-$BaSnO_3$ microwave dielectrics, Ceram. Int. 26 (2000) 57–62.
[17] L. Chai, P.K. Davies, Formation and structural characterization of 1:1 ordered perovskites in the $BaZn_{1/3}Ta_{2/3}O_3$-$BaZrO_3$ system, J. Am. Ceram. Soc. 80 (1997) 3193–3198.
[18] K. Kageyama, Crystal structure and microwave dielectric properties of $BaZn_{1/3}Ta_{2/3}O_3$-$(Sr,Ba)(Ga_{1/2}Ta_{1/2})O_3$ ceramics, J. Am. Ceram. Soc. 75 (1992) 1767–1771.
[19] J.-I. Yang, C.-H. Choi, H.-J. Lee, H.-M. Park, Microstructure and microwave dielectric properties of $BaZn_{1/3}Ta_{2/3}O_3$ ceramics with ZrO_2 addition, J. Am. Ceram. Soc. 85 (2002) 165–168.
[20] S.J. Webb, J. Breeze, R.I. Scott, D.S. Cannell, D.M. Iddles, N.M. Alford, Raman spectroscopic study of gallium-doped $BaZn_{1/3}Ta_{2/3}O_3$, J. Am. Ceram. Soc. 85 (2002) 1753–1756.
[21] H. Wu, P.K. Davies, Influence of non-stoichiometry on the structure and properties of $BaZn_{1/3}Nb_{2/3}O_3$ microwave dielectrics: II. Compositional variations in pure BZN, J. Am. Ceram. Soc. 89 (2006) 2250–2263.
[22] T. Kolodiazhnyi, Origin of extrinsic dielectric loss in 1:2 ordered, single-phase $BaMg_{1/3}Ta_{2/3}O_3$, J. Eur. Ceram. Soc. 34 (2014) 1741–1753.
[23] S. Zhang, H. Sahin, E. Torun, F. Peeters, D. Martien, T. DaPron, N. Dilley, N. Newman, Fundamental mechanisms responsible for the temperature coefficient of resonant frequency in microwave dielectric ceramics, J. Am. Ceram. Soc. 100 (2017) 1508–1516.
[24] S. Kawashima, M. Nishida, I. Ueda, H. Ouchi, $Ba(Zn_{1/3}Ta_{2/3}O_3)$ ceramics with low dielectric loss at microwave frequencies, J. Am. Ceram. Soc. 66 (1983) 421–423.
[25] S.B. Desu, H.M. O'Bryan, Microwave loss quality of $BaZn_{1/3}Ta_{2/3}O_3$ ceramics, J. Am. Ceram. Soc. 68 (1985) 546–551.
[26] T.A. Vanderah, E. Pickett, I. Levin, R.S. Roth, Ternary subsolidus for the system BaO–ZnO–Ta_2O_5. NIST Phase Equilibria Diagrams Fig. 11283, (2001).
[27] V.G. Kryshtop, R.U. Devlikanova, V.S. Filip'ev, E.G. Fesenko, Crystal-chemical conditions for the existence of complex oxides of the $A_6B_{10}O_{30}$ type with tetragonal potassium-tungsten bronze structure, Inorg. Mater. 19 (1983) 945–948.
[28] V. Tolmer, G. Desgardin, Low-temperature sintering and influence of the process on the dielectric properties of $BaZn_{1/3}Ta_{2/3}O_3$, J. Am. Ceram. Soc. 80 (1997) 1981–1991.
[29] S.M. Moussa, J.B. Claridge, M.J. Rosseinsky, S. Clarke, R.M. Ibberson, T. Price, D.M. Iddles, D.C. Sinclair, $Ba_8ZnTa_6O_{24}$: a high-Q microwave dielectric from a potentially diverse homologous series, Appl. Phys. Lett. 82 (2003) 4537–4539.
[30] L.M. Kovba, L.N. Lykova, M.V. Paromova, L.M. Lopato, A.V. Shevchenko, Barium oxide-tantalum oxide system, Zhurnal Neorg. Khimii 22 (1977) 2845–2847.
[31] L.M. Kovba, L.N. Lykova, M.V. Paromova, Z.Ya. Pol'shchikova, Polymorphism of barium tantalate $Ba_6Ta_2O_{11}$, Zhurnal Neorg. Khimii 22 (1977) 2584–2586.
[32] T.A. Vanderah, R.S. Roth, T. Siegrist, W. Febo, J.M. Loezos, W. Wong-Ng, Subsolidus phase equilibria and crystal chemistry in the system BaO–TiO_2–Ta_2O_5, Solid State Sci. 5 (2003) 149–164.
[33] V. Petricek, M. Dusek, L. Palatinus, Crystallographic computing system JANA2006: general features, Z. Kristallogr. 229 (2014) 345–352.
[34] I.M. Reaney, P.L. Wise, I. Qazi, C.A. Miller, T.J. Price, D.S. Cannell, D.M. Iddles, M.J. Rosseinsky, S.M. Moussa, M. Bieringer, L.D. Noailles, Ordering and quality factor in 0.95 $BaZn_{1/3}Ta_{2/3}O_3$-0.05$SrGa_{1/2}Ta_{1/2}O_3$ production resonators, J. Eur. Ceram. Soc. 23 (2003) 3021–3034.
[35] A.J. Jacobson, B.M. Collins, B.E.F. Fender, A powder neutron and X-ray diffraction determination of the structure of $Ba_3Ta_2ZnO_9$: an investigation of perovskite phases in the system Ba-Ta-Zn-O and the preparation of $Ba_2TaCdO_{5.5}$ and $Ba_2CeInO_{5.5}$, Acta Crystallogr. B32 (1976) 1083–1087.
[36] V.H.G. von Schnering, R. Hoppe, J. Zemann, Die Kristallstruktur des $BaZnO_2$, Z. Anorg. Allg. Chem 305 (1960) 241–254.
[37] Supplementary Information.
[38] M.W. Lufaso, Crystal structures, modeling, and dielectric property relationships of 2:1 ordered $Ba_3MM'_2O_9$ (M = Mg, Ni, Zn; M′ = Nb, Ta) perovskites, Chem. Mater. 16 (2004) 2148–2156.
[39] M. Bieringer, S.M. Moussa, L.D. Noailles, A. Burrows, C.J. Kiely, M.J. Rosseinsky, R.M. Ibberson, Cation ordering, domain growth, and zinc loss in the microwave dielectric oxide $Ba_3ZnTa_2O_{9-\delta}$, Chem. Mater. 15 (2003) 586–597.
[40] H. Tamura, D.A. Sagala, K. Wakino, Lattice vibrations of $BaZn_{1/3}Ta_{2/3}O_3$ crystal with ordered perovskite structure, Jpn. J. Appl. Phys. 25 (1986) 787–791.
[41] C.-T. Chia, Y.-C. Chen, H.-F. Cheng, Correlation of microwave dielectric properties and normal vibration modes of $xBa(Mg_{1/3}Ta_{2/3})O_3$-$(1-x)Ba(Mg_{1/3}Nb_{2/3})O_3$ ceramics: I. Raman spectroscopy, J. Appl. Phys. 94 (2003) 3360–3364.
[42] I.G. Siny, R. Tao, R.S. Katiyar, R. Guo, A.S. Bhalla, Raman spectroscopy of Mg–Ta order–disorder in $BaMg_{1/3}Ta_{2/3}O_3$, J. Phys. Chem. Solids 59 (1998) 181–195.
[43] C.-C. Lee, C.-C. Chou, D.-S. Tsai, Effect of La/K A-site substitution on the ordering of $BaZn_{1/3}Ta_{2/3}O_3$, J. Am. Ceram. Soc. 80 (1997) 2885–2890.
[44] Y.-I. Kim, Synthesis, Crystal Structures, and Dielectric Property of Oxynitride Perovskites (Ph.D. dissertation), Ohio State University, 2005.
[45] G. Rong, N. Newman, B. Shaw, D. Cronin, Role of Ni and Zr doping on the electrical, optical, magnetic, and structural properties of barium zinc tantalate ceramics, J. Mater. Res. 14 (1999) 4011–4019.